

High-rate precise point positioning (PPP) to measure seismic wave motions: an experimental comparison of GPS PPP with inertial measurement units

Peiliang Xu · Chuang Shi · Rongxin Fang ·
Jingnan Liu · Xiaoji Niu · Quan Zhang ·
Takashi Yanagidani

Received: 18 August 2011 / Accepted: 23 November 2012 / Published online: 9 December 2012
© Springer-Verlag Berlin Heidelberg 2012

Abstract High-rate GPS has been widely used to construct displacement waveforms and to invert for source parameters of earthquakes. Almost all works on internal and external evaluation of high-rate GPS accuracy are based on GPS relative positioning. We build an experimental platform to externally evaluate the accuracy of 50-Hz PPP displacement waveforms. Since the shake table allows motion in any of six degrees of freedom, we install an inertial measurement unit (IMU) to measure the attitude of the platform and transform the IMU displacements into the GPS coordinate system. The experimental results have shown that high-rate PPP can produce absolute horizontal displacement waveforms at the accuracy of 2–4 mm and absolute vertical displacement waveforms at the sub-centimeter level of accuracy within a short period of time. The significance of the experiments indicates that high-rate PPP is capable of detecting absolute seismic displacement waveforms at the same high accuracy as GPS relative positioning techniques, but requires no fixed datum station. We have also found a small scaling error of IMU and a small time offset of misalignment between high-rate PPP and IMU displacement waveforms by comparing the amplitudes of and cross-correlating both the displacement waveforms.

Keywords Displacement waveforms · High-rate GPS · IMU · Precise point positioning (PPP) · Seismic wave motion

P. Xu · T. Yanagidani
Disaster Prevention Research Institute,
Kyoto University, Uji., Kyoto 611-0011, Japan
e-mail: pxu@rcep.dpri.kyoto-u.ac.jp

C. Shi (✉) · R. Fang · J. Liu · X. Niu · Q. Zhang
GNSS Research Center, Wuhan University,
Wuhan, 430071, People's Republic of China
e-mail: shi@whu.edu.cn

1 Introduction

Space GNSS/GPS technology has been routinely used to precisely measure crustal deformation (see, e.g., Prescott et al. 1989; Shimada et al. 1990) since GPS was first successfully demonstrated to estimate baseline components at the cm level of accuracy more than three decades ago (see, e.g., Counselman and Shapiro 1979; MacDoran 1979; Bossler et al. 1980). In particular, significant advances in GPS hardware and data processing have enabled GPS measurements at a very high frequency. Accordingly, we can obtain a time series of precise positions of an object in motion (see, e.g., Nikolaidis et al. 2001; Bock et al. 2004), which has resulted in an interdisciplinary subject of study, namely GPS seismology. GPS seismology uses GPS as displacement seismometers/instruments at a high sampling rate for earthquake study (see, e.g., Larson 2009). The major advantages of GPS seismometers are: (i) they can measure arbitrarily large dynamic displacements without saturation (see, e.g., Bock et al. 2004). In other words, with GPS seismometers, we do not need to worry that displacements are too large to go beyond the measurement range of GPS and cannot be correctly recorded, as otherwise inherent with conventional seismometers; and (ii) GPS-derived displacements are free of instrumental drift, clipping due to instrumental tilts and rotations that are inherited with seismometers (see, e.g., Genrich and Bock 2006; Emore et al. 2007; Graizer 2009, 2010). However, GPS is a few orders of magnitudes less sensitive than seismometers, in the sense that GPS can only detect movements at the noise level of a few millimeters or accelerations at the noise level of sub-centimeter per second squared (see, e.g., Salazar et al. 2011), while seismometers are able to sense accelerations at the noise level of 10^{-6} millimeter per second squared in the frequency range between 0.001 and 0.2 Hz (see, e.g., Wielandt and Streckeisen 1982; Clinton 2004).

Thus, GPS and seismometers can complement each other in both sensitivity and large dynamic displacements.

Although the sampling interval of 30 s served almost as a standard format to collect GPS data at permanent stations for deformation measurement, Larson et al. (2003) first successfully detected the high-rate GPS waveforms of displacements caused by the 3 November 2002 Mw7.9 Denali Fault earthquake by using relative GPS positioning techniques to process the 1-Hz GPS data. Kouba (2003, 2005) first applied GPS precise point positioning (PPP) to process the high-rate GPS data for the 2002 Denali Fault and 2004 great Sumatra–Andaman earthquakes and obtained the corresponding waveforms of displacements at a number of IGS stations. Recently, Colosimo et al. (2011) proposed using the time difference technique and standard GPS broadcast products to position a single receiver in real time and demonstrated centimeter level of positioning accuracy with 1 and 5 Hz dual frequency carrier phase data. Subsequent works provide more successful examples of the measurement of displacement wave motions from different earthquakes (see, e.g., Bock et al. 2004; Ohta et al. 2006; Bilich et al. 2008; Shi et al. 2010; Avallone et al. 2011), combine high-rate GPS with strong motion seismographs and propose filtering and smoothing techniques to further improve the accuracy of relative displacement waveforms (see, e.g., Emore et al. 2007; Wang et al. 2007; Bilich et al. 2008; Davis and Smalley 2009; Bock et al. 2011) and to invert for source parameters of slip distribution and seismic moment from high-rate GPS waveforms of displacements (see, e.g., Ji et al. 2004; Ohta et al. 2008; Yokota et al. 2009; Avallone et al. 2011; Melgar et al. 2012; Crowell et al. 2012). For clarity, we may distinguish high-rate GPS from kinematic GPS. By high-rate GPS, we mean GPS precise positioning within a short period of time (say, a few minutes) with a high sampling rate, e.g., 50 Hz in this study, after ambiguity resolution or after the convergence of floating solutions of coordinates. In the case of kinematic GPS, we are generally concerned more about the performance of real-time GPS precise positioning in a long term (say tens of minutes to days) with a variety of sampling rates from seconds to minutes or even longer, depending on specific applications of interest.

The accuracy of high-rate displacement waveforms derived from GPS has been reported in the literature through internal and external comparisons. By *internal* and *external* comparisons, we mean that the accuracy of GPS displacement waveforms is derived from analyzing GPS (observed minus estimated) residuals of carrier phase data only and by comparing the GPS-only displacement results with those from instruments other than GPS such as strong motion seismometers, respectively. Remondi (1985) demonstrated that kinematic positioning at the centimeter level of accuracy can be obtained in seconds by applying difference methods to process GPS carrier phase data. Genrich and Bock (2006) used instantaneous geodetic positioning to analyze 10- to

50-Hz GPS measurements. By removing outliers, which can range from 1.8 to 16.8 % (Bock et al. 2000), and by averaging the positions over a number of epochs, Genrich and Bock (2006) reported that relative positioning accuracy for baselines up to 10 km can be from 1.1 to 5.8 mm in the east component, 1.4 to 7.6 mm in the north component, and 3.4 to 43.7 mm in the vertical component. By averaging 20-Hz data into 2-Hz data, the accuracy can even be as high as 0.5 mm in the horizontal components and 3–4 mm in the vertical component. Nevertheless, for baselines longer than 39 km, the accuracy is worsened to 6.1–8.1 mm in the east component, 6.9–9.9 mm in the north component and 38.6–51.8 mm in the vertical component. Since averaging data may significantly distort displacement waveforms, the high accuracy by averaging may not apply to high-rate GPS displacements. Bilich et al. (2008) reported that the accuracy of horizontal components was about 4.0–10 mm and that of the vertical component about 10–20 mm. Ohta et al. (2008) showed that the internal PPP accuracy of positions was 5.2 mm in the east component, 4.3 mm in the north component and 10.4 mm in the vertical component. Since wide-lane ambiguities and phase biases are freely available for most of the IGS global GPS stations, Bertiger et al. (2010) proposed using these data to constrain local ambiguities at a local station of interest. They showed with GPS data at the sampling interval of 30 s that after the ambiguity resolution, kinematic solutions of a single point positioning can be repeated at the level of 7.7, 8.4 and 11.7 mm in the east, north and vertical components, respectively. The accuracy of high-rate GPS displacements was also confirmed by comparing them with those from strong motion seismographs in a nearby seismic station (see, e.g., Bock et al. 2004; Ohta et al. 2006; Wang et al. 2007; Bilich et al. 2008; Bock et al. 2011).

However, only a few works have conducted external quality evaluation of high-rate GPS displacement waveforms by comparison with results from instruments other than GPS. Ge et al. (2000) conducted an experiment with both GPS antenna and seismometers installed on a shaking simulator. By processing 20-Hz GPS data in a relative positioning mode, with a reference station being about 10 m away from the simulator, they reported that the accuracy of the high-rate GPS-derived displacements was about 20 mm in the horizontal components and 30 mm in the vertical component. Elósegui et al. (2006) evaluated the accuracy of GPS-derived displacements by installing a GPS antenna on a very precise, one-dimensionally displaced shake table. Since the shake table can only be displaced in one direction, they analyzed the north component data and reported an accuracy of about 2.5 mm for 1-Hz GPS-derived relative displacements over a baseline of 10 m. Ning et al. (2009) used a controlled robot arm to evaluate the accuracy of 20 Hz GPS displacements and concluded from the two baselines of 400 m and 60 km that the accuracy of the relative displacements are 3.5 mm

in the east component, 5.6 mm in the north component and 8.1 mm in the vertical component. While this paper is under revision, thanks to one of the reviewers, we are brought to the attention of the work by [Bock et al. \(2011\)](#), which showed with the uniaxial large high-performance shake table that the accuracy of displacements by GPS relative positioning with a nearby reference station can be as good as 2.6–4.0 mm. When the GPS displacements are combined with those from seismometers, the accuracy of combined displacements can be further improved ([Bock et al. 2011](#)).

Although there exist a large number of reports on the integration of GPS and inertial navigation systems, their major focus is on use of low-cost IMU to aid in GPS navigation and enhance the reliability of such integrated navigation systems, in particular, in the case of GPS outages, for anti-jamming or when GPS measurements are not available to position (see, e.g., [Farrell et al. 2000](#); [Wendel et al. 2006](#); [Naranjo et al. 2009](#); [Hwang et al. 2011](#)). Since navigation will generally last for a long time, no performance evaluation of such systems over a short period of time, e.g., within a few minutes, has been reported. In this study, our major purpose is to investigate the accuracy of high-rate PPP to measure seismic wave motion over a short period of time, say, up to a few minutes. We will show that high-rate PPP displacement waveforms can reach millimeter accuracy in the horizontal components and sub-centimeter accuracy in the vertical component within a short period of time without any reference or fixed station.

2 Design of high-rate GPS/IMU experiments

The current external evaluations of the accuracy of GPS-derived displacement waveforms ([Ge et al. 2000](#); [Elósegui et al. 2006](#); [Ning et al. 2009](#)) are obviously based on GPS relative positioning with a reference station located nearby. In practical seismic observations on a large earthquake, a fixed reference station is undesirable (see, e.g., [Davis and Smalley 2009](#)), since relative positioning results do not contain any information on whether the reference station moves or not during the earthquake. Although a very short baseline can be determined very precisely, it is not practically useful in field seismic observations. As for a long baseline, further work may be required to check whether the high accuracy reported by [Ning et al. \(2009\)](#) can be attained routinely, because high accuracy of long baselines is generally not warranted, as can be seen in [Genrich and Bock \(2006\)](#). Except for [Ge et al. \(2000\)](#); [Elósegui et al. \(2006\)](#) and [Ning et al. \(2009\)](#) used precise robot arms instead of seismometers to externally assess the GPS-derived displacement waveforms. Although relative positioning has always been used to externally evaluate the accuracy of high-rate GPS seismometers ([Ge et al. 2000](#); [Elósegui et al. 2006](#); [Ning et al. 2009](#)), bearing in mind that PPP technology would become a key technique to measure

dynamical deformation, the purpose of this research is to investigate how precisely high-rate PPP can measure seismic wave motions.

A large earthquake may generate large strong motions in the frequency range between 0.01 and 10 or 20 Hz ([Shibutani 2012](#), personal communication). As is well known, GPS is a powerful tool to precisely measure static or dynamic displacements. Therefore, to evaluate the accuracy of high-rate PPP positioning, we will attempt to simulate real-life seismic observations in the case of a large earthquake and conduct a new external evaluation of the accuracy of high-rate GPS PPP displacement waveforms. More precisely, we design new external experiments by fully taking into account the following four factors:

- (i) *Datum*: In the case of large earthquakes, it may not be reasonable to assume a fixed reference station without any displacement (see, e.g., [Davis and Smalley 2009](#)). Thus, it is highly desirable to process GPS data in practice by using GPS PPP techniques. Bearing in mind that all external evaluations of high-rate GPS displacement waveforms are based on GPS relative positioning with a fixed datum ([Ge et al. 2000](#); [Elósegui et al. 2006](#); [Ning et al. 2009](#)), we decide to process GPS data in the PPP mode and conduct external evaluation of the accuracy of high-rate PPP displacement waveforms in this new experiment.
- (ii) *Problems in seismic observation*: When seismometers are set up for observation, they may not be correctly aligned to the local reference frame. In addition, they may be subject to tilts and rotations in the recording of large earthquakes, as theoretically discussed by [Graizer \(2009, 2010\)](#) and practically observed, e.g., by [Takeo \(2009\)](#). However, since a triaxial seismometer is actually an inertial measurement unit (IMU) with only three degrees of freedom on translational motion, it lacks three more degrees of freedom on rotational motion to correct the effect of tilts and rotations. Thus, we decide to directly use a fully operational IMU in our experiment.
- (iii) *Sampling rate*: Although 1-Hz GPS data have been routinely recorded and used in seismological study (see, e.g., [Larson et al. 2003](#); [Kouba 2003](#)), [Smalley \(2009\)](#) suggested that sampling at 10 Hz be required to obtain aliasing-free observations close to the fault for M7 and larger earthquakes. [Genrich and Bock \(2006\)](#) collected GPS data up to 50 Hz and obtained sub-millimeters of accuracy by averaging data of many epochs. Because the averaging process will automatically mix up the displacement signals, we will directly examine the accuracy of independent 50-Hz epoch-by-epoch PPP displacement waveforms. More specially, we use Trimble Net R8 receiver and sample GPS data at 50 Hz in the experiment. The antenna for Trimble Net R8 receiver

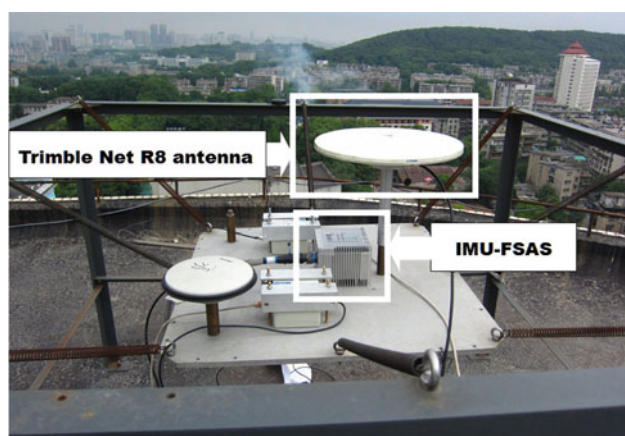


Fig. 1 The experiment platform with the shake table, Trimble Net R8 antenna and IMU

has embedded choke rings to mitigate the effect of multipath.

- (iv) *Shake table*: Bearing in mind that earthquakes could cause motions in all six degrees of freedom (see, e.g., Graizer 2009, 2010; Takeo 2009), we design a more flexible shake table to allow motion in all six degrees of freedom in the experiment, instead of precisely controlling movements in one direction and/or translationally (see, e.g., Elósegui et al. 2006; Ning et al. 2009; Bock et al. 2011). The shake table is tightened to a fixed frame with eight springs. By changing the springs with different stiffness, we can also readily change the frequency of the shake table.

The experiment platform with these four factors materialized has been constructed on the roof of a 16-story building inside the Campus of Wuhan University and is shown in Fig. 1. We may note that this 16-story building is one of the tallest buildings in its surrounding.

3 PPP and IMU data processing

With the experiment platform shown in Fig. 1, we push the shake table to move and conduct a number of experiments. The states and ranges of motion of the shake table can be readily manipulated by pushing and/or pulling it along different directions. Trimble Net R8 antenna/receiver on the platform records GPS data at the sampling rate of 50 Hz and the IMU collects the three-dimensional attitudes of the platform and the three-dimensional accelerations at the sampling rate of 200 Hz. The GPS data from Trimble Net R8 antenna/receiver on the shake table are processed in the PPP mode by using the software package PANDA for Positioning And Navigation Data Analyst, which was developed by the

GNSS Research Center, Wuhan University (see, e.g., Liu and Ge 2003; Shi et al. 2008).

Like other popular GPS software systems such as GIPSY and GAMIT, PANDA is a powerful and multi-functional GPS software system, which can be used for precise orbit determination, adjustment of GPS CORS networks, GPS baseline processing and PPP. For the purpose of this experimental research, we only use the PPP component of PANDA. The basic equations of PANDA for PPP are ionospheric-free combinations of dual frequency P-code and carrier phase observables. Although there are a number of different weighting schemes in the literature (see, e.g., Eueler and Goad 1991; Dach et al. 2007), PANDA implements the following elevation-dependent formula

$$w(A_e) = \begin{cases} 1, & \text{if } A_e > 30^\circ \\ 2 \sin(A_e), & \text{if } A_e \leq 30^\circ, \end{cases} \quad (1)$$

to determine the weights of ionospheric-free observables, where A_e is the elevation angle. PANDA also follows the IERS conventions 2003 to correct tidal effects and antenna phase center. Tropospheric delays are corrected using the Saastamoinen model with the global mapping function of Boehm et al. (2006). Residual zenith total delays are approximated by a random walk process with prior constraint of 10 cm on its initial state. For each continuously tracked orbital arc, we assume one ambiguity. Station coordinates and receiver clock errors are estimated epoch by epoch.

We set the cutoff angle to 7° . We also use the IGS final precise orbit and 5-s satellite clock products. At this moment, PANDA does not implement the function to fix ambiguities in the PPP mode. In other words, we PPP-solve the positions of the GPS antenna by using floating solutions only. In general, the solution of coordinates for a static station will take about 25 min of data to converge. The parameters of interest are the absolute displacement waveforms of the GPS antenna, which are independently estimated epoch by epoch by using the weighted least squares method. By *absolute displacements*, we mean that they can be determined without reference to any fixed station.

In our experiments, we use an IMU-FSAS inertial measurement unit made by iMAR GmbH, Germany, which consists of three closed-loop fiber-optic gyros and three servo accelerometers. According to the specifications from the manufacturer, the IMU measures the attitudes of the platform with the accuracy of about $29''$, $29''$ and $43''$ for roll, pitch and yaw, respectively. In order to compare the PPP displacements with those from the IMU, we integrate the accelerations twice to obtain the displacement waveforms. Since the measurements by the IMU unit are all taken on the body frame, we have to use the attitudes of roll, pitch and yaw from the IMU output and transform the displacements from the IMU body frame into the local coordinate system. All

these computations are performed by using the software system provided by the instrument maker. Although we asked for technical details on the software system, we did not get them from the manufacturer for commercial reasons. Nevertheless, to get some (even rough) idea on the noise level of the IMU, we select two almost linear segments from the IMU displacement waveforms collected on 2 April 2011 for each of the three coordinate components, fit the IMU displacements to straight lines and use the fit residuals to compute the standard deviations. The standard deviations obtained are 1.151 and 1.329 mm in the east component, 0.831 and 0.829 mm in the north component and, finally, 0.686 and 0.440 mm in the vertical component, respectively.

Because the IMU is not collocated exactly with the Trimble Net R8 antenna, we have to further convert the coordinates collected by the IMU to those at the site of the GPS antenna such that the displacements from both the GPS PPP and the IMU are exactly in the same local coordinate system and exactly at the same location. Given the series of GPS coordinates $\mathbf{x}_t = (x_t, y_t, z_t)$ and the initial coordinates $\mathbf{x}_0 = (x_0, y_0, z_0)$ at the site of the GPS antenna, we can transform them into the coordinates in the local east, north and vertical (ENU) system through the following formula

$$\begin{bmatrix} E_t \\ N_t \\ U_t \end{bmatrix} = \begin{bmatrix} -\sin(L_t) & \cos(L_t) & 0 \\ -\sin(B_t)\cos(L_t) & -\sin(B_t)\sin(L_t) & \cos(B_t) \\ \cos(B_t)\cos(L_t) & \cos(B_t)\sin(L_t) & \sin(B_t) \end{bmatrix} \begin{bmatrix} x_t - x_0 \\ y_t - y_0 \\ z_t - z_0 \end{bmatrix}, \quad (2)$$

where (E_t, N_t, U_t) stands for the coordinates at the time t in the local east, north and vertical system (see e.g., [Grewal et al. 2001](#)), (L_t, B_t) the geodetic longitude and latitude at the time t . To convert the ENU coordinates at the IMU site into those at the site of the GPS antenna, we have to assume the initial vector from the IMU unit to the GPS antenna at the body frame, which is measured before the experiments are started. More precisely speaking, the ENU coordinates at the GPS site computed from the IMU measurements are computed by using the following formula

$$\begin{bmatrix} E_t^{i2g} \\ N_t^{i2g} \\ U_t^{i2g} \end{bmatrix} = \begin{bmatrix} E_t^{imu} \\ N_t^{imu} \\ U_t^{imu} \end{bmatrix} + \begin{bmatrix} \mathbf{1}_E^T \\ \mathbf{1}_N^T \\ \mathbf{1}_U^T \end{bmatrix} \delta \mathbf{b}, \quad (3)$$

where $\delta \mathbf{b}$ is the initial vector from the IMU to the GPS antenna in the body frame and measured before the experiments are started, $(E_t^{i2g}, N_t^{i2g}, U_t^{i2g})$ stands for the ENU coordinates at the GPS site computed from the IMU measurements, $(E_t^{imu}, N_t^{imu}, U_t^{imu})$ for the ENU coordinates of the IMU, and the three unit vectors $\mathbf{1}_E, \mathbf{1}_N$ and $\mathbf{1}_U$ are given as follows (see also [Grewal et al. 2001](#)):

$$\mathbf{1}_E = \begin{bmatrix} \sin(\psi_t)\cos(\theta_t) \\ \cos(\phi_t)\cos(\psi_t) + \sin(\phi_t)\sin(\psi_t)\sin(\theta_t) \\ -\sin(\phi_t)\cos(\psi_t) + \cos(\phi_t)\sin(\psi_t)\sin(\theta_t) \end{bmatrix}, \quad (4a)$$

$$\mathbf{1}_N = \begin{bmatrix} \cos(\psi_t)\cos(\theta_t) \\ \cos(\phi_t)\sin(\psi_t) + \sin(\phi_t)\cos(\psi_t)\sin(\theta_t) \\ \sin(\phi_t)\sin(\psi_t) + \cos(\phi_t)\cos(\psi_t)\sin(\theta_t) \end{bmatrix}, \quad (4b)$$

$$\mathbf{1}_U = \begin{bmatrix} \sin(\theta_t) \\ -\sin(\phi_t)\cos(\theta_t) \\ -\cos(\phi_t)\cos(\theta_t) \end{bmatrix}, \quad (4c)$$

where ϕ_t, θ_t and ψ_t stand for the roll, pitch and yaw at the time epoch t , respectively.

Since an IMU device is essentially a strong motion seismometer with six degrees of freedom, we expect the same problem of distortions and shifts of a seismometer, as well described and explained in [Boore and Bommer \(2005\)](#). As a result, we apply the piecewise linear baseline correction technique of [Boore and Bommer \(2005\)](#) to correct the IMU-derived displacement waveforms. For more techniques of baseline correction with nonlinear functions, the reader is referred to [Boore and Bommer \(2005\)](#). A consequence of baseline correction is that long-term trends of displacements and permanent offsets are removed and cannot be recovered from IMU data. We note that the IMU has a small scale factor error. Because GPS measurements have never been reported to have any scaling problem, we adjust the IMU scale factor to GPS and apply the corresponding corrections to obtain the final IMU-derived displacement waveforms.

4 Experimental results and discussions

We have conducted a number of experiments to compare the displacement waveforms from the 50-Hz PPP and the 200-Hz IMU. In this paper, we will focus on the experiment conducted on 2 April 2011. The satellite geometry and the corresponding horizontal and vertical DOP (Dilution Of Precision) values, namely, HDOP and VDOP, are shown in [Fig. 2](#) with a minimum cutoff elevation angle of 7° . Most of the time, we have nine satellites for positioning. Since the satellite PRN18 is of a low elevation angle, it is neither shown in [Fig. 2](#) nor used in the HDOP/VDOP computations. It is clear from [Fig. 2](#) that the HDOP values are between 1.01 and 1.26, and the VDOP values between 1.81 and 2.59; both the HDOP and VDOP values indicate that the satellite geometry is excellent during the experiments. The VDOP values are roughly larger than those of HDOP by a factor of two throughout the experiment.

During the experiment on 2 April 2011, we placed the platform in motion several times after collecting the GPS data in static mode for about 50 min. As a result, we obtained several sets of PPP and IMU displacement waveforms. Without applying any corrections to the IMU-output displacements, we simply subtracted the IMU displacements from the corresponding PPP displacements. Since we observe the same behaviour among all the differences in any of the east, north

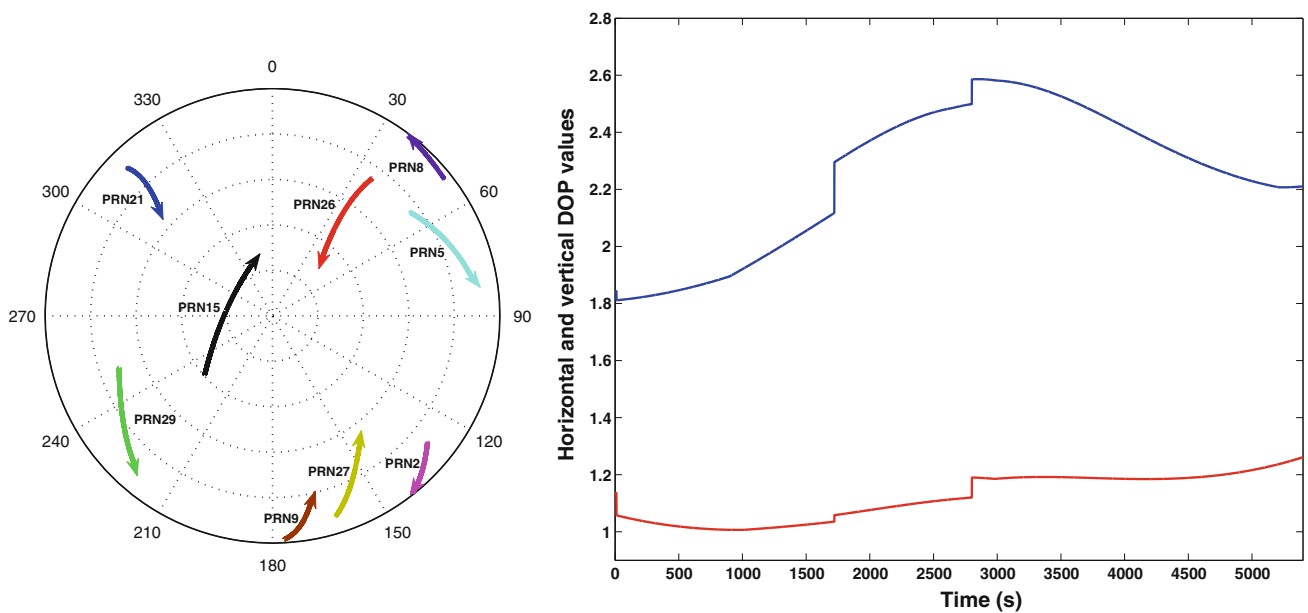
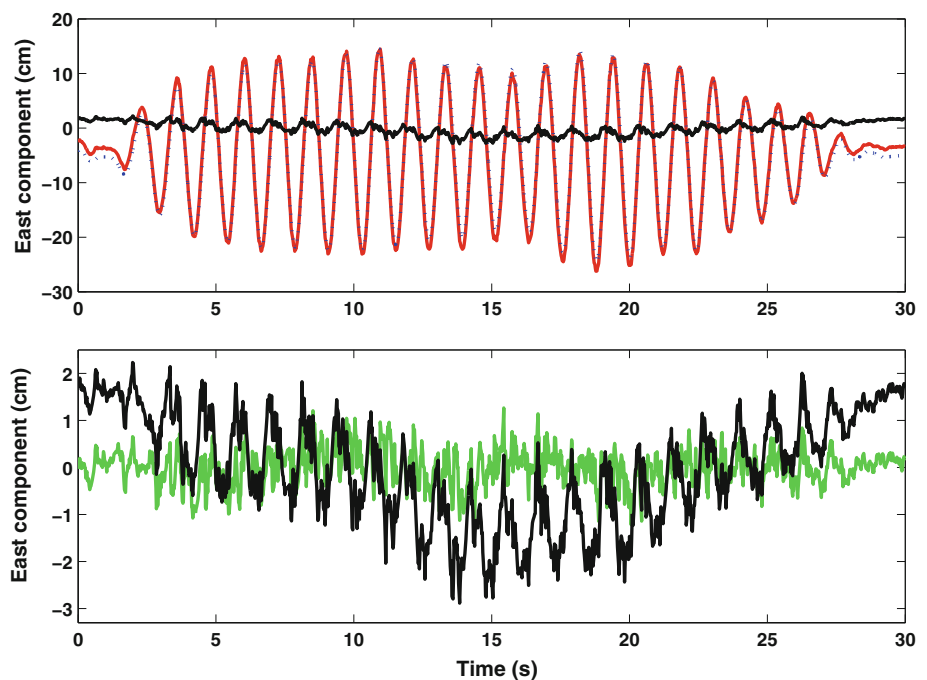


Fig. 2 The GPS satellite geometry and the horizontal and vertical DOP values during the experiments. *The left plot*—the GPS satellite distribution in the sky, with the *arrows* showing the trajectories of the GPS satellites; *the right plot*—the horizontal (*red line*) and vertical (*blue line*) DOP values

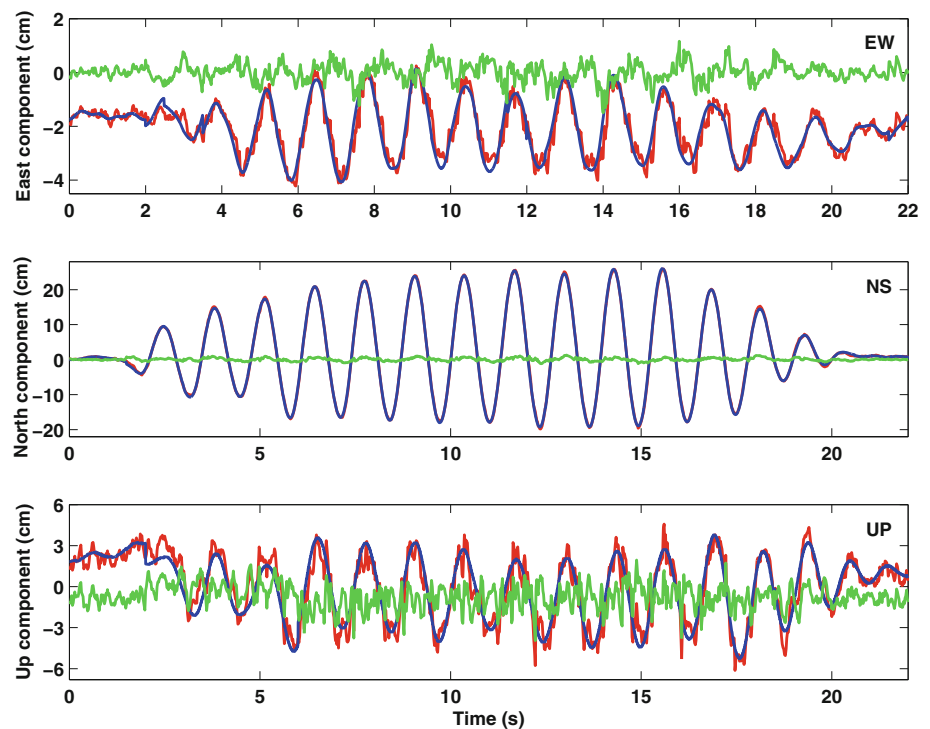
Fig. 3 Displacement wave motions directly computed from PPP and IMU without any corrections. *The upper plot*—the PPP-computed (*red line*) and IMU-output (*blue-dotted line*) displacement wave motions in the east component, together with the errors or differences (*black line*) between the PPP-computed and IMU-output displacements without any corrections; *the lower plot*—showing the *black line* in the above panel in a larger scale (*black line*). Also plotted in this lower panel are the errors or differences (*green line*) between the PPP-computed and IMU-derived displacements after baseline and other corrections are applied to the IMU displacements



and vertical components, we only show one segment in the east component in Fig. 3. We can clearly observe two features from Fig. 3: (i) In the upper panel, although PPP and IMU displacement waveforms appear to match very well, their difference (black line) clearly shows a wave motion signal, with the same period as those of PPP and IMU displacement waveforms, but with a much smaller magnitude. From the physical point of view, this should indicate that the PPP and IMU displacement waveforms have a small shift

of phase. Since both GPS and IMU observe the same wave motion, such a small shift should imply that GPS timing and IMU timing do not match exactly. Thus, we cross-correlate PPP and IMU waveforms and find a 0.01-s time shift for correction to be applied to all the IMU-output displacements. Actually, since the sampling rate of the IMU is 200 Hz, the corresponding time increment is 0.005 s. As a result, we can left- and/or right-shift the IMU displacement waveform on the basis of this minimum time increment, cross-correlate

Fig. 4 The displacement waveforms from PPP (red line) and IMU (blue line) and their corresponding differences in displacements between PPP and IMU (green line): *the upper panel*—the east component; *the middle panel*—the north component; and *the lower panel*—the vertical component



the shifted IMU waveform with the PPP displacement waveform and output the time offset/shift when the maximum correlation coefficient is attained. (ii) The black line in the lower panel clearly shows piecewise linear trends, which have been often reported to be due to distortions, tilts and shifts in the literature of seismology and earthquake engineering (see e.g., [Boore and Bommer 2005](#)). This lower panel also clearly indicates that baseline correction must be applied to the IMU-derived displacement waveforms. We follow [Boore and Bommer \(2005\)](#) and use piecewise linear functions for baseline correction. The errors with correlation and baseline corrections are then shown in the green line, which has a much smaller magnitude but still exhibits some wave signals. This latter phenomenon is due to the fact that because of the limit of IMU sampling rate (200 Hz), we can only find the minimum time shift of 0.005 s from cross-correlation.

With the importance of the above corrections in mind, we investigate whether IMU might have any problem in scaling. In order to determine the IMU scaling relative to GPS, we sum up the absolute values of all the displacements in the east and north components, induced by shaking the platform and derived from PPP and IMU, which are denoted by d_{GPS} and d_{IMU} , respectively. As a result, we can determine the single scaling factor $s = d_{\text{GPS}}/d_{\text{IMU}}$ for all the experiments on 2 April 2011 to correct the IMU-derived displacements. The value of s is equal to 1.0248. The displacements in the vertical components are not used in the computation of the scaling, because GPS vertical components are of poor accuracy. Thus, we finally apply all the correlation, baseline and

scaling corrections to the IMU-derived displacements at the site of GPS antenna for comparison with PPP displacements in the remainder of this paper. More specifically, we obtain four to six displacement waveforms for each of the east, north and vertical components. One set of displacements is plotted in Fig. 4. The differences in displacements between PPP and IMU are also shown in Fig. 4 in green lines. It is obvious from the red and blue lines of Fig. 4 that the displacement waveforms from PPP match those from IMU very well, as can also be confirmed by the green lines of displacement errors between PPP and IMU. The errors in the horizontal components are much smaller than those in the vertical component. It is also clear from Fig. 4 that the lines from the IMU look much smoother than those from GPS PPP, which may indicate that the noise of IMU is smaller than PPP. A small signal wave motion can also be seen from this figure, again, due to the fact that we cannot resolve a time shift better than the sampling limit of the IMU from the correlation of PPP and IMU displacements, as explained above. Two more sets of displacements for each component are shown in Fig. 5, with PPP in red lines and IMU in blue dotted lines. The results are consistent with those reported in Fig. 4 and provide strong support of the fact that both PPP and IMU displacements match very well.

Based on the differences in the displacement waveforms between PPP and IMU, we then compute the accuracy of displacement differences, which are listed in Table 1, with the first three columns corresponding to Figs. 4 and 5, respectively. The displacement waveforms from PPP differ those

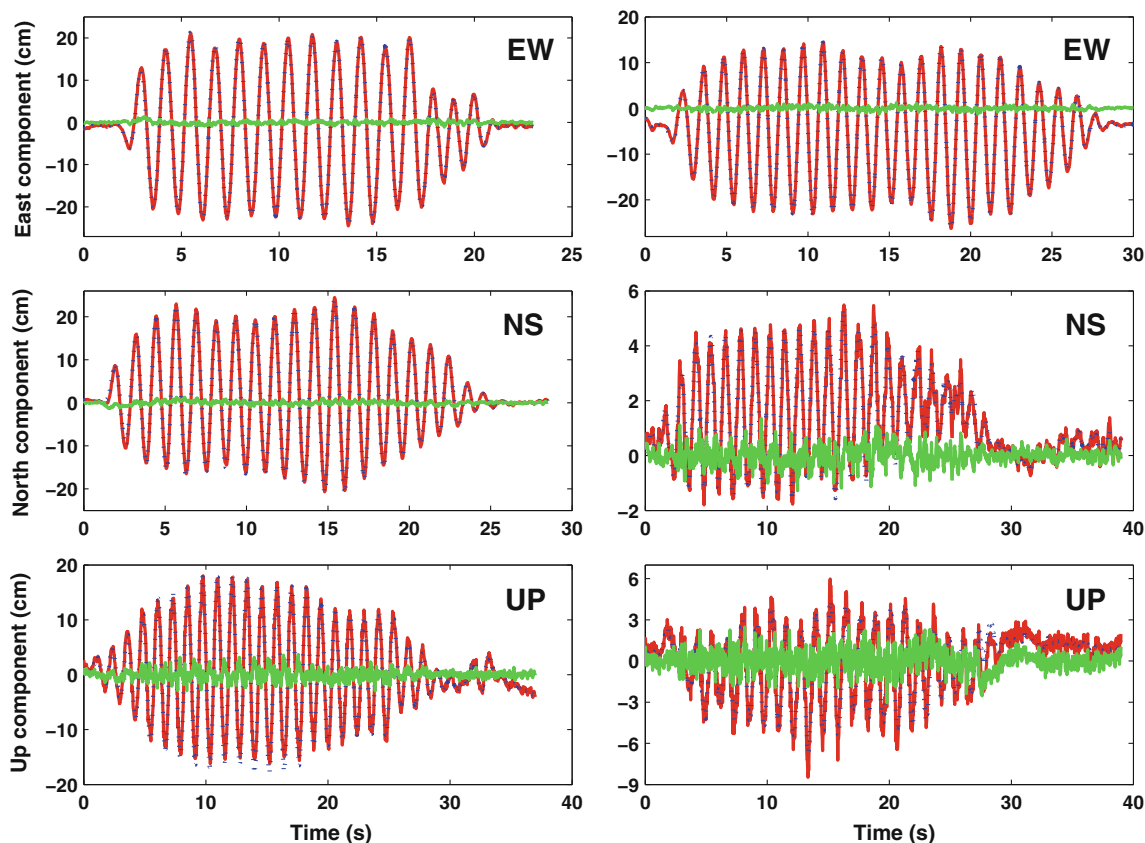


Fig. 5 The displacement waveforms from PPP (red line) and IMU (blue dotted line) and their corresponding differences in displacements between PPP and IMU (green line): the upper panels—the east component; the middle panels—the north component; and the lower panels—the vertical component

from IMU in the horizontal components within a standard deviation of 2.76–4.17 mm. The accuracy of displacement differences in the vertical component is between 7.31 and 9.07 mm, which is worse than those in the horizontal components by about a factor of two. Based on the accuracy results in Table 1, we can compute the ratios of the accuracy in the vertical component to the horizontal accuracy, with both the east and north components being taken into account, which are equal to 2.02, 1.66, 1.51 and 1.83 for the four examples in the table, respectively. Since all these examples are experimented between 3,000 and 4,000 s in the DOP plot of Fig. 2, we can see that these ratios are very close to the mean value 2.10 of VDOP/HDOP over the time interval [3,000, 4,000]. Although it is widely accepted that PPP is less precise than GPS relative positioning techniques (see, e.g., Davis and Smalley 2009), the accuracy results in Table 1 clearly indicate that high-rate PPP is as precise as high-rate relative positioning, when compared with the external experiments by Elósegui et al. (2006) and Ning et al. (2009). Actually, the accuracy results in Table 1 are even better than GPS internal accuracy evaluation in relative positioning mode, e.g., by Bock et al. (2000, 2004) and Bilich et al. (2008). The external experiments also clearly indicate that high-rate

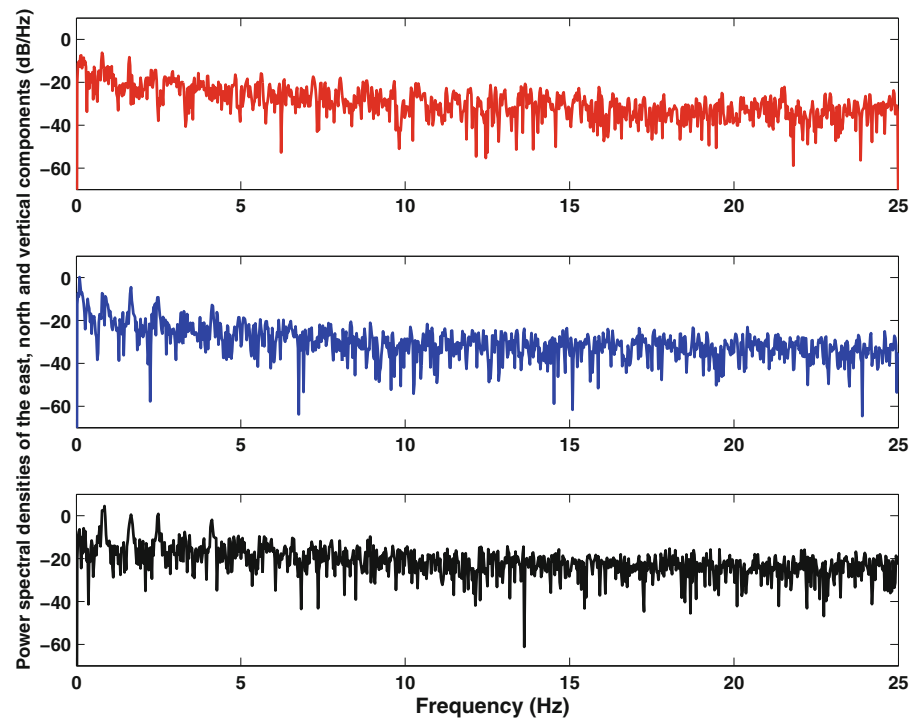
Table 1 Accuracy of displacement differences between PPP and IMU (mm)

Experiment examples	1	2	3	4
East	3.10	3.55	3.62	2.76
North	3.14	4.07	3.22	4.17
Vertical	8.89	8.95	7.31	9.07

PPP can accurately detect absolute millimeter-horizontal and centimeter-vertical displacement waveforms, respectively.

To further study the nature of displacement errors, we compute the power spectral densities (PSD) of the differences of the three displacement waveforms between PPP and IMU shown on the left side of Fig. 5, which are plotted in Fig. 6. The PSD values shown in the vertical axis in dB/Hz are computed by the transformation $10 \log_{10}(\text{PSD cm}^2)$. Roughly speaking, the three PSD curves look more or less flat, though they show slightly stronger power values up to 10 Hz. To be more precise, we fit the PSD values of all the three components to the power law f^β , where f is the frequency and β is to be estimated. The values of β are equal to 0.198, 0.174 and 0.201 for the east, north and vertical components,

Fig. 6 Power spectral densities of the displacement errors between PPP and IMU: *upper panel (red line)*—the east component; *middle panel (blue line)*—the north component; and *lower panel (black line)*—the vertical component. In this figure, $\text{dB} = 10 \log_{10}(\text{PSD cm}^2)$



respectively. Obviously, these values are not very far away from zero. From this point of view, we may say that the displacement errors between PPP and IMU are roughly of white noise nature. At least, these errors are much closer to white noise than to noise of other types, with $\beta = -2, -1, 1$ and 2 , respectively, standing for red, pink, blue and violet noises. The white noise behavior of high-rate displacement errors here is consistent with that of high-rate relative positioning of short baselines reported by [Genrich and Bock \(2006\)](#). It is also clear from [Fig. 6](#) that the powers of the displacement errors in the vertical component are much stronger or larger than those in the horizontal components (compare the blue line with the red and green lines), which is consistent with the accuracy results in [Table 1](#). Nevertheless, we can still see three to four peaks in the frequency range between 0 and 5 Hz, in particular, in the north and vertical components. We do not find any sources of errors to explain them.

The above comparison between high-rate PPP and IMU has clearly shown that high-rate PPP can accurately detect wave motions at the millimeter level of accuracy in the horizontal component and at the sub-centimeter level of accuracy in the vertical component within a short period of time. Even though currently PANDA PPP does not fix the ambiguity unknowns to their integers, these accuracy results are still better than the repeatability of kinematic precise point solutions with ambiguity constraints reported by [Bertiger et al. \(2010\)](#). This phenomenon could further imply that high-rate PPP can be powerful to remove more errors, which may behave like systematic errors within minutes, but otherwise

show random nature in kinematic precise point solutions over a long time of, say, tens of minutes to days. Thus, we will further show the performance of high-rate PPP in static mode within a short period of time. In other words, we keep the experiment platform motionless, but use the PPP software to process the collected GPS data as if the platform were shaken or in motion. Actually, the first several tens of minutes of GPS data in our experiment on 2 April satisfies this requirement exactly. Thus, we randomly or arbitrarily take five segments of GPS data, each with a length of 3 min, to demonstrate the performance of PPP errors in static mode. Shown in [Fig. 7](#) are the error performances of two static PPP examples: one with a 1-min length of data and the other with a 3-min length of data. Note, however, that for clarity, we shift the mean values of the east, north and vertical components by 10, 30 and 50 cm, respectively. With these five segments of 3-min data, we can also compute the standard deviations for all the three components, which are listed in [Table 2](#). With these standard deviations, we also compute the mean value of VDOP/HDOP for these five examples. Actually, the mean VDOP/HDOP value is equal to 1.542 in the case of 1-min data and 1.538 in the case of 3-min data, both of which are quite close to the mean VDOP/HDOP value of 1.893 computed from the first half hour of GPS satellite geometry (compare [Fig. 2](#)).

The standard deviations in [Table 2](#) clearly indicate that high-rate static PPP can reach millimeter level of accuracy for both the horizontal and vertical components and can be as precise as daily relative positioning solutions. We should warn, however, that these results are only valid for high-rate

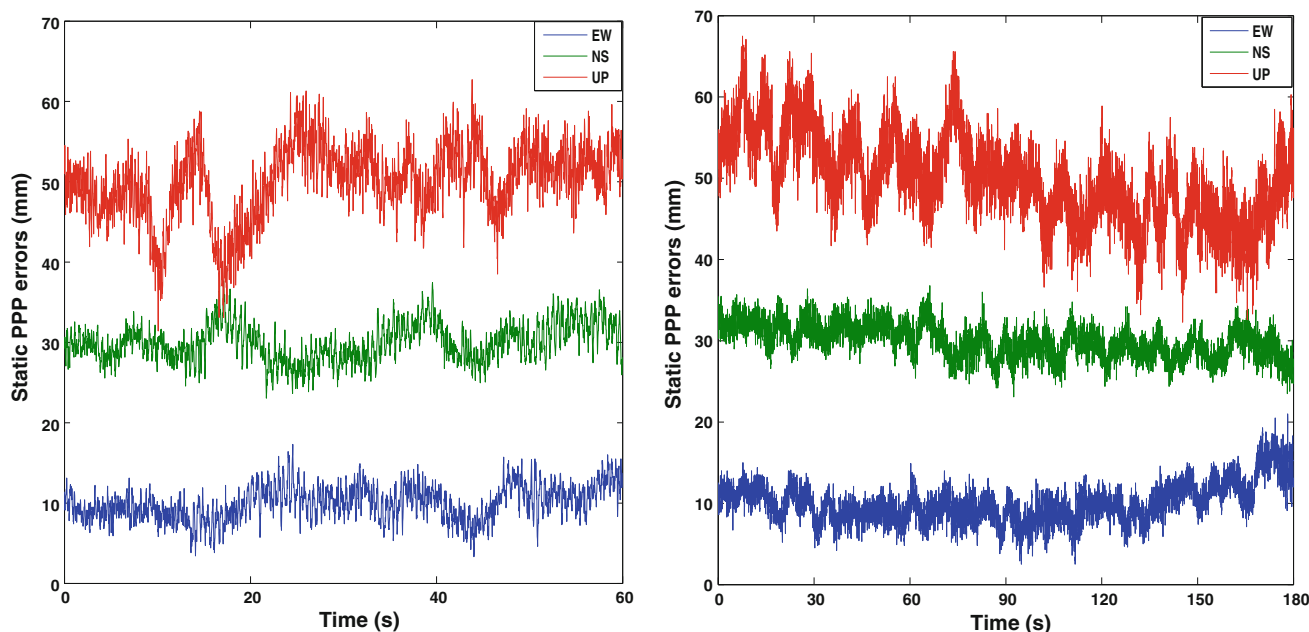


Fig. 7 The error performances of static PPP in the east (blue line), north (green line) and vertical (red line) components. *The left plot*—with 1 min of GPS data; *the right plot*—with 3 min of GPS data

Table 2 The standard deviations of static PPP errors (mm)

Experiment examples	1	2	3	4	5
1 min data					
East	2.14	2.00	2.44	2.15	1.80
North	2.39	2.49	2.31	2.07	1.49
Vertical	4.57	4.19	5.40	4.42	4.41
3 min data					
East	2.49	3.38	2.22	3.21	2.40
North	2.42	2.36	2.71	3.11	2.10
Vertical	4.41	7.42	6.38	4.83	5.48

PPP over a short time of minutes. When comparing a high-rate static PPP solution with the daily relative positioning solution, an offset can be exhibited. However, high-rate PPP over a short period of time is particularly advantageous for applications where precise positioning information over a short time is fundamental. Such applications include, for example, the measurement of seismic wave motions, volcano eruption, storm wind (or earthquake)-induced deformation of sky-high building or tower, and safety monitoring of large bridges and dams. When high-rate PPP technology is applied to CORS stations and/or Japanese GEONET, all the GPS stations will automatically serve as displacement seismometers.

Table 2 also confirms the above experimental results of millimeter level of accuracy obtained from the comparison between high-rate PPP and IMU. When comparing the standard deviations in Table 2 with those in Table 1, we see that

the errors of static PPP performs better than those from the comparison between PPP and IMU. There may be three reasons for this: (i) the standard deviations in Table 1 contain both errors from both GPS and IMU; (ii) PPP positioning with the platform in motion could be also affected by the changing environment conditions such as multipath, which, otherwise, remain unchanged in the case of static PPP; and (iii) the process of converting IMU accelerations to displacements and its inherent problems.

5 Concluding remarks

High-rate precise relative GNSS positioning has become a key technology in earth sciences and civil engineering. In GNSS seismology, however, a fixed datum is neither available nor desirable, since an absolute determination of seismic wave motion is fundamental to invert for the source physics of an earthquake (see, e.g., Aki and Richards 2002). Although PPP techniques have been reported to have mm to cm level of accuracy in static mode (see, e.g., Ge et al. 2008; Kouba and Héroux 2001), to our best knowledge, no external experimental comparison of PPP with other independent instruments has previously been reported to understand the error nature of high-rate PPP within a short period of time. In this paper, we have designed such an experimental platform and conducted a number of experiments to compare the absolute waveforms of motion by 50-Hz PPP with those from an inertial measurement unit. The results have clearly demonstrated that high-rate PPP can achieve an accuracy of 2–4 mm in the

horizontal components and a sub-centimeter accuracy in the vertical component within a short period of time, indicating that high-rate PPP is capable of detecting seismic wave motion with an amplitude of sub-centimeter horizontally and/or 1.5–2.0 cm vertically with a confidence level of 95 %. The experimental results obtained in this paper immediately imply the feasibility of precisely measuring an absolute seismic waveform in GPS seismology, potential applications of real-time tsunami monitoring for hazard prediction and mitigation, and real-time safety monitoring of structures in civil engineering, all at the accuracy of millimeter level horizontally and sub-centimeter level vertically.

Acknowledgments The authors are very grateful to the reviewers, the associate editor, Prof. J. Kusche, and the Editor-in-Chief, Prof. R. Klees, for their very constructive comments and for bringing a few articles on the topic, just published or in press, to the attention of the authors while this paper was under review, which have resulted in a significant improvement of the presentation of the paper. They are also grateful to one of the reviewers for polishing the English of the text. This work is partially supported by the National Natural Science Foundation of China (Projects 41104024, 41174028 and 41231174) and the 111 Project B07037, PRC Ministry of Education. Finally, the authors are also grateful to Prof. T. Shibutani, a seismologist at Kyoto University, for personal communication on 7 Nov 2012 about frequency range of strong motions in the case of large earthquakes.

References

- Aki K, Richards PG (2002) Quantitative seismology, 2nd edn. University Science Books, California
- Avallone A, Marzario M, Cirella A, Piatanesi A, Rovelli A, Alessandro CD, D'Anastasio E, D'Agostino N, Giuliani R, Mattone M (2011) Very high rate (10Hz) GPS seismology for moderate-magnitude earthquakes: the case of the Mw6.3 L'Aquila (central Italy) event. *J Geophys Res* 116:B02305. doi:10.1029/2010JB007834
- Bertiger W, Desai SD, Haines B, Harvey E, Moore AW, Owen S, Weiss JP (2010) Single receiver phase ambiguity resolution with GPS data. *J Geod* 84:327–337
- Bilich A, Cassidy JF, Larson KM (2008) GPS seismology: application to the 2002 Mw7.9 Denali Fault earthquake. *Bull Seismol Soc Am* 98:593–606
- Bock Y, Nikolaidis RM, de Jonge PJ (2000) Instantaneous geodetic positioning at medium distances with the Global Positioning System. *J Geophys Res* 116(B12):28223–28253
- Bock Y, Prawirodirdjo L, Melbourne TI (2004) Detection of arbitrarily large dynamic ground motions with a dense high-rate GPS network. *Geophys Res Lett* 31:L06604. doi:10.1029/2003GL019150
- Bock Y, Melgar D, Crowell BW (2011) Real-time strong-motion broadband displacements from collocated gps and accelerometers. *Bull Seismol Soc Am* 101:2904–2925
- Boehm J, Niell A, Tregoning P, Schuh H (2006) Global Mapping Function (GMF): a new empirical mapping function based on numerical weather model data. *Geophys Res Lett* 33:L07304
- Boore DM, Bommer JJ (2005) Processing of strong-motion accelerograms: needs, options and consequences. *Soil Dynam Earthq Eng* 25:93–115
- Bossler JD, Goad CC, Bender PL (1980) Using the Global Positioning System (GPS) for geodetic positioning. *Bull Géod* 54:553–563
- Clinton JF (2004) Modern digital seismology—instrumentation, and small amplitude studies in the engineering world, PhD thesis, California Institute of Technology, Pasadena, California
- Colosimo G, Crespi M, Mazzoni A (2011) Real-time GPS seismology with a stand-alone receiver: a preliminary feasibility demonstration. *J Geophys Res* 116:B11302. doi:10.1029/2010JB007941
- Counselman CC, Shapiro II (1979) Miniature interferometer terminals for Earth surveying. *Bull Géod* 53:139–163
- Crowell BW, Bock Y, Melgar D (2012) Real-time inversion of GPS data for finite fault modeling and rapid hazard assessment. *Geophys Res Lett* 39:L09305. doi:10.1029/2012GL051318
- Dach R, Hugentobler U, Fridez P, Meindl M (2007) Bernese GPS software version 5.0. Astronomical Institute, University of Bern, Bern
- Davis JP, Smalley R Jr (2009) Love wave dispersion in central North America determined using absolute displacement seismograms from high-rate GPS. *J Geophys Res* 114:B11303. doi:10.1029/2009JB006288
- Elósegui P, Davis JL, Oberlander D, Baena R, Ekström G (2006) Accuracy of high-rate GPS for seismology. *Geophys Res Lett* 33:L11308. doi:10.1029/2006GL026065
- Emore GL, Haase JS, Choi K, Larson KM, Yamagiwa A (2007) Recovering seismic displacements through combined use of 1-Hz GPS and strong-motion accelerometers. *Bull Seismol Soc Am* 97:357–378
- Euler H, Goad CC (1991) On optimal filtering of GPS dual frequency observations without using orbit information. *Bull Géod* 65:130–143
- Farrell JA, Givargis TD, Barth MJ (2000) Real-time differential carrier phase GPS-aided INS. *IEEE Trans Control Syst Technol* 8:709–721
- Genrich JF, Bock Y (2006) Instantaneous geodetic positioning with 10–50 Hz GPS measurements: Noise characteristics and implications for monitoring networks. *J Geophys Res* 111:B03403. doi:10.1029/2005JB003617
- Graizer V (2009) Tutorial on measuring rotations using multipendulum systems. *Bull Seismol Soc Am* 99:1064–1072
- Graizer V (2010) Strong motion recordings and residual displacements: what are we actually recording in strong motion seismology? *Seismol Res Lett* 81:635–639
- Ge L, Han S, Rizos C, Ishikawa Y, Hoshiba M, Yoshida Y, Izawa M, Hashimoto N, Himori S (2000) GPS seismometers with up to 20 Hz sampling rate. *Earth Planets Space* 52:881–884
- Ge MR, Gendt G, Rothacher M, Shi C, Liu J (2008) Resolution of GPS carrier-phase ambiguities in precise point positioning (PPP) with daily observations. *J Geod* 82:389–399
- Grewal MS, Weill LR, Andrews AP (2001) Global positioning systems, inertial navigation and integration. Wiley, New York
- Hwang DH, Lim DW, Cho SL, Lee SJ (2011) Unified approach to ultra-tightly-coupled GPS/INS integrated navigation system. *IEEE AE Syst Mag* 2011:30–38
- Ji C, Larson KM, Tan Y, Hudnut KW, Choi K (2004) Slip history of the 2003 San Simon earthquake constrained by combining 1-Hz GPS, strong motion, and teleseismic data. *Geophys Res Lett* 31:L17608. doi:10.1029/2004GL020448
- Kouba J (2003) Measuring seismic waves induced by large earthquakes with GPS. *Stud Geophys Geod* 47:741–755
- Kouba J (2005) A possible detection of the 26 December 2004 great Sumatra-Andaman islands earthquake with solution products of the international GNSS service. *Stud Geophys Geod* 49:463–483
- Kouba J, Héroux P (2001) Precise point positioning using IGS orbits and products. *GPS Solut* 5:12–28
- Larson KM (2009) GPS seismology. *J Geod* 83:227–233
- Larson KM, Bodin P, Gombert J (2003) Using 1-Hz GPS data to measure deformations caused by the Denali fault earthquake. *Science* 300:1421–1424
- Liu J, Ge M (2003) PANDA software and its preliminary result of positioning and orbit determination. *J Nat Sci Wuhan Univ* 8(2B):603609. doi:10.1007/BF02899825

- MacDoran PF (1979) Satellite emission radio interferometric Earth surveying series—GPS geodetic system. *Bull Géod* 53:117–138
- Melgar D, Bock Y, Crowell B (2012) Real-time centroid moment tensor determination for large earthquakes from local and regional displacement records. *Geophys J Int* 188:703–718. doi:[10.1111/j.1365-246X.2011.05297.x](https://doi.org/10.1111/j.1365-246X.2011.05297.x)
- Nikolaidis RM, Bock Y, de Jonge PJ, Shearer P, Agnew DC, van Donseelaar M (2001) Seismic wave observations with the Global Positioning System. *J Geophys Res* 106(B10):21897–21916
- Ning T, Johansson JM, Scherneck H-G, Jarlemark POJ, Ewardson R (2009) High-rate GNSS techniques for the detection of large seismic displacements. In: Proceedings of IGARSS2009, July 12–17, Cape Town, South, Africa, pp V359–V362
- Naranjo JE, Jiménez F, Aparicio F, Zato J (2009) GPS and inertial systems for high precision positioning on motorways. *J Navigation* 62:351–363
- Ohta Y, Meilano I, Sagiya T, Kimata F, Hirahara K (2006) Large surface wave of the 2004 Sumatra-Andaman earthquake captured by the very long baseline kinematic analysis of 1-Hz GPS data. *Earth Planets Space* 58:153–157
- Ohta Y, Ohzono M, Miura S, Inuma T, Tachibana K, Takatsuka K, Miyao K, Sato T, Umino N (2008) Coseismic fault model of the 2008 Iwate-Miyagi Nairiku earthquake deduced by a dense GPS network. *Earth Planets Space* 60:1197–1201
- Prescott WH, Davis JL, Svarc JL (1989) Global Positioning System measurements for crustal deformation: precision and accuracy. *Science* 244:1337–1340
- Remondi BW (1985) Performing centimeter-level surveys in seconds with GPS carrier phase: initial results. *Navigation* 32:386–400
- Salazar D, Hernandez-Pajares M, Juan-Zornoza JM, Sanz-Subirana J, Aragon-Angel A (2011) EVA: GPS-based extended velocity and acceleration determination. *J Geod* 85:329–340
- Shi C, Zhao Q, Geng J, Lou Y, Ge M, Liu J (2008) Recent development of PANDA software in GNSS data processing. In: Proceedings of the Society of Photographic Instrumentation Engineers, 7285, 72851S. doi:[10.1117/12.816261](https://doi.org/10.1117/12.816261)
- Shi C, Lou Y, Zhang H, Zhao Q, Geng J, Wang R, Fang R, Liu J (2010) Seismic deformation of the Mw8.0 Wenchuan earthquake from high-rate GPS observations. *Adv Space Res* 46:228–235
- Shimada S, Fujinawa Y, Sekiguchi S, Ohmi S, Eguchi T, Okada Y (1990) Detection of a volcanic fracture opening in Japan using Global Positioning System measurements. *Nature* 343:631–633
- Smalley R Jr (2009) High-rate GPS: how high do we need to go? *Seism Res Lett* 80:1054–1061
- Takeo M (2009) Rotational motions observed during an earthquake swarm in April 1998 Offshore Ito, Japan. *Bull Seismol Soc Am* 99:1457–1467
- Wang G, Boore DM, Tang G, Zhou X (2007) Comparisons of ground motions from collocated and closely spaced one-sample-per-second Global Positioning System and accelerograph recordings of the 2003 M6.5 San Simon, California, earthquake in the Parkfield region. *Bull Seismol Soc Am* 97:76–90
- Wendel J, Meister O, Schlaile C, Trommer CF (2006) An integrated GPS/MEMS-IMU navigation system for an autonomous helicopter. *Aerosp Sci Technol* 10:527–533
- Wielandt E, Streckeisen G (1982) The leaf-spring seismometer: design and performance. *Bull Seismol Soc Am* 72:2349–2367
- Yokota Y, Koketsu K, Hikima K, Miyazaki S (2009) Ability of 1-Hz GPS data to infer the source process of a medium-sized earthquake: the case of the 2008 Iwate-Miyagi Nairiku, Japan, earthquake. *Geophys Res Lett* 36:L12301. doi:[10.1029/2009GL037799](https://doi.org/10.1029/2009GL037799)